

# nature materials



MAY 2011 VOL 10 NO 5  
[www.nature.com/naturematerials](http://www.nature.com/naturematerials)

## MICROFLUIDICS

Drop control

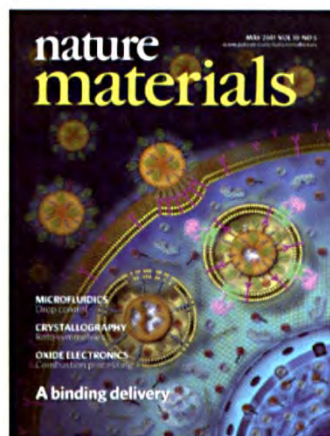
## CRYSTALLOGRAPHY

Roto symmetries

## OXIDE ELECTRONICS

Combustion processing

# A binding delivery



### COVER IMAGE

A nanocarrier — synthesized by the fusion of liposomes to spherical, nanoporous silica particles and by subsequent modification of the lipid bilayer with targeting peptides and fusogenic peptides — shows the targeted delivery and controlled release of chemically diverse multicomponent cargos within the cytosol of human liver carcinoma cells.

Article p389; News & Views p342

# The targeted delivery of multicomponent cargos to cancer cells by nanoporous particle-supported lipid bilayers

Carlee E. Ashley<sup>1\*</sup>†, Eric C. Carnes<sup>2</sup>, Genevieve K. Phillips<sup>3</sup>, David Padilla<sup>1</sup>, Paul N. Durfee<sup>4</sup>, Page A. Brown<sup>5</sup>, Tracey N. Hanna<sup>6</sup>, Juewen Liu<sup>1†</sup>, Brandy Phillips<sup>3</sup>, Mark B. Carter<sup>3</sup>, Nick J. Carroll<sup>2</sup>, Xingmao Jiang<sup>1</sup>, Darren R. Dunphy<sup>1</sup>, Cheryl L. Willman<sup>3,7</sup>, Dimiter N. Petsev<sup>2</sup>, Deborah G. Evans<sup>5</sup>, Atul N. Parikh<sup>8</sup>, Bryce Chackerian<sup>3,4</sup>, Walker Wharton<sup>3,7</sup>, David S. Peabody<sup>3,4</sup> and C. Jeffrey Brinker<sup>1,2,3,4,9\*</sup>

**Encapsulation of drugs within nanocarriers that selectively target malignant cells promises to mitigate side effects of conventional chemotherapy and to enable delivery of the unique drug combinations needed for personalized medicine. To realize this potential, however, targeted nanocarriers must simultaneously overcome multiple challenges, including specificity, stability and a high capacity for disparate cargos. Here we report porous nanoparticle-supported lipid bilayers (protocells) that synergistically combine properties of liposomes and nanoporous particles. Protocells modified with a targeting peptide that binds to human hepatocellular carcinoma exhibit a 10,000-fold greater affinity for human hepatocellular carcinoma than for hepatocytes, endothelial cells or immune cells. Furthermore, protocells can be loaded with combinations of therapeutic (drugs, small interfering RNA and toxins) and diagnostic (quantum dots) agents and modified to promote endosomal escape and nuclear accumulation of selected cargos. The enormous capacity of the high-surface-area nanoporous core combined with the enhanced targeting efficacy enabled by the fluid supported lipid bilayer enable a single protocell loaded with a drug cocktail to kill a drug-resistant human hepatocellular carcinoma cell, representing a 10<sup>6</sup>-fold improvement over comparable liposomes.**

Targeted delivery of drugs encapsulated within nanocarriers<sup>1,2</sup> can overcome problems exhibited by conventional ‘free’ drugs, including poor solubility, limited stability, rapid clearing and, in particular, lack of selectivity, which results in nonspecific toxicity to normal cells<sup>3</sup> and prevents the dose escalation necessary to eradicate malignant cells<sup>4</sup>. Passive targeting schemes rely on the enhanced permeability of tumour vasculature and the decreased draining efficacy of tumour lymphatics (the so-called enhanced permeability and retention effect<sup>5,6</sup>) to direct accumulation of nanocarriers at tumour sites, but the lack of cell-specific interactions needed to induce nanocarrier internalization decreases therapeutic efficacy and can result in drug expulsion and induction of multiple drug resistance (MDR; ref. 7). Furthermore, not all tumours exhibit the enhanced permeability and retention effect<sup>5,6</sup>, and passively targeted nanocarriers are no more effective at treating blood cancers than free drugs<sup>8</sup>. Selective targeting strategies employ ligands that specifically interact with receptors expressed on the cell surface of interest to promote nanocarrier binding and internalization<sup>9</sup>. This strategy requires that receptors are highly overexpressed by cancer cells (10<sup>4</sup>–10<sup>5</sup> copies/cell)

relative to normal cells to maximize selectivity and therapeutic efficacy<sup>1</sup>. Multiple copies of a targeting ligand can be conjugated to the nanocarrier surface to promote multivalent binding effects<sup>10</sup>, which result in enhanced affinity<sup>11</sup> and more efficient drug delivery through receptor-mediated internalization pathways that help circumvent MDR efflux mechanisms<sup>12</sup>. However, high ligand densities can promote nonspecific interactions with endothelial and other non-cancerous cells and increase immunogenicity, resulting in opsonization-mediated clearance of nanocarriers<sup>13</sup>. Modifying the nanocarrier surface with hydrophilic polymers, such as polyethylene glycol (PEG), increases circulation times by reducing interactions with serum proteins and mitigating uptake by phagocytic cells; such strategies invariably reduce targeting specificity, however<sup>13</sup>. The main challenge for targeted nanocarriers is to simultaneously achieve high targeting specificity and delivery efficiency, while avoiding nonspecific binding and entrapment by the body’s defences.

Here we report a new class of nanocarrier that synergistically combines features of mesoporous silica particles<sup>14–19</sup> and liposomes<sup>20–22</sup> to address the multiple challenges of targeted

<sup>1</sup>Center for Micro-Engineered Materials, University of New Mexico, Albuquerque, New Mexico 87131, USA, <sup>2</sup>Department of Chemical and Nuclear Engineering, University of New Mexico, Albuquerque, New Mexico 87131, USA, <sup>3</sup>Cancer Research and Treatment Center, University of New Mexico, Albuquerque, New Mexico 87131, USA, <sup>4</sup>Department of Molecular Genetics and Microbiology, University of New Mexico, Albuquerque, New Mexico 87131, USA, <sup>5</sup>Department of Chemistry, University of New Mexico, Albuquerque, New Mexico 87131, USA, <sup>6</sup>Department of Chemical Engineering, University of Florida, Gainesville, Florida 32611, USA, <sup>7</sup>School of Medicine, Department of Pathology, University of New Mexico, Albuquerque, New Mexico 87131, USA, <sup>8</sup>Department of Applied Science, University of California Davis, Davis, California 95616, USA, <sup>9</sup>Self-Assembled Materials Department, Sandia National Laboratories, Albuquerque, New Mexico 87185-1349, USA. †Present addresses: Harry S. Truman Post-Doctoral Fellow; Biotechnology and Bioengineering Department, Sandia National Laboratories, Livermore, California 94551, USA (C.E.A.); Department of Chemistry, University of Waterloo, Waterloo, Ontario, N2L 3G1, Canada (J.L.). \*e-mail: ceashle@sandia.gov; cjbrink@sandia.gov.

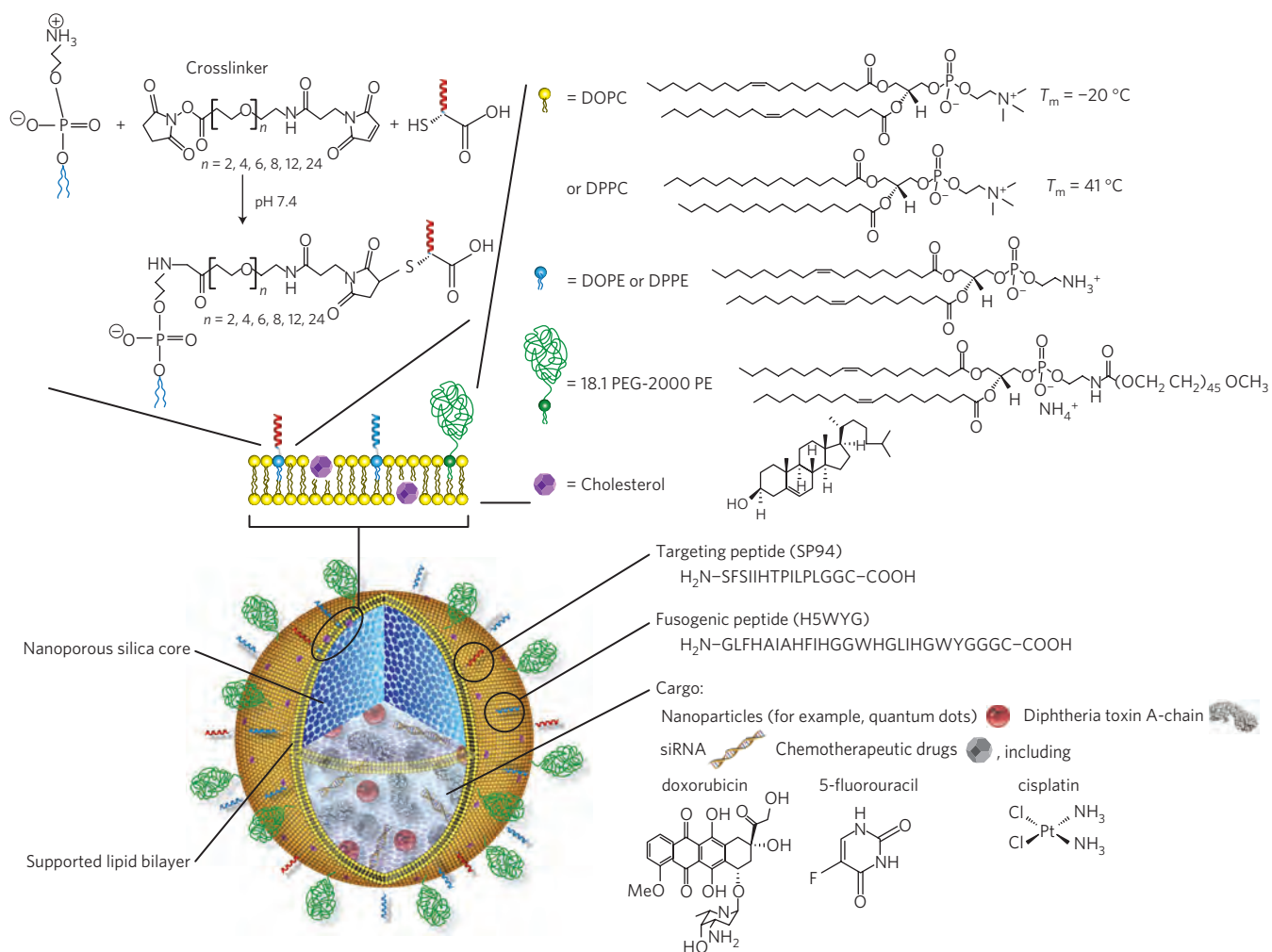


**Figure 1 | Schematic illustration of the nanoporous particle-supported lipid bilayer, depicting the disparate types of therapeutic and diagnostic agent that can be loaded within the nanoporous silica core, as well as the ligands that can be displayed on the surface of the SLB.** Targeting and fusogenic peptides are chemically conjugated to phosphatidylethanolamine (DOPE or DPPC), present in the SLB at 1–5 wt%, by a heterobifunctional crosslinker with a PEG spacer arm ( $n = 24$ ). The SLB, composed of either fluid (DOPC) or non-fluid (DPPC) zwitterionic phosphatidylcholine lipids with 30 wt% cholesterol, is further modified with 5 wt% PEG-2000 PE to enhance colloidal stability and decrease nonspecific interactions.

delivery. Fusion of liposomes to a spherical, high-surface-area, nanoporous silica core<sup>23–26</sup>, followed by modification of the resulting supported lipid bilayer (SLB) with multiple copies of a targeting peptide, a fusogenic peptide and PEG results in a nanocarrier construct (the ‘protocell’) that, compared with liposomes, the most extensively studied class of nanocarriers<sup>20–22</sup>, improves on capacity, selectivity and stability and enables targeted delivery and controlled release of high concentrations of multicomponent cargos within the cytosol of cancer cells (see Fig. 1 and Supplementary Methods for experimental details). Specifically, owing to its high surface area ( $>1,000\text{ m}^2\text{ g}^{-1}$ ), the nanoporous silica core (Fig. 2a) possesses a higher capacity for therapeutic and diagnostic agents than similarly sized liposomes. Furthermore, owing to substrate–membrane adhesion energy, the core suppresses large-scale bilayer fluctuations (see Supplementary Fig. S3a and refs 27–32), resulting in greater stability than unsupported liposomal bilayers. Interestingly, the nanoporous support also results in enhanced lateral bilayer fluidity compared with that of either liposomes or SLBs formed on non-porous particles. As we shall demonstrate, this synergistic combination of materials and biophysical properties enables high delivery efficiency and enhanced targeting specificity with a minimal number of targeting ligands, features crucial to maximizing specific

binding, minimizing nonspecific binding, reducing dosage and mitigating immunogenicity.

Protocells are synthesized by liposome fusion to high-surface-area spherical silica particles characterized by an isotropic, worm-like nanoporosity (see Fig. 2a and Supplementary Fig. S1). To demonstrate that SLBs formed on particles with surface-accessible nanopores have unique long-range fluidity, we carried out temperature-dependent fluorescence recovery after photobleaching (FRAP) of DPPC bilayers supported on either a nanoporous or solid (that is non-porous) silica particle (see Fig. 2b). We observe that fluorescence in the photobleached region begins to recover abruptly at  $35^\circ\text{C}$  ( $\pm 1^\circ\text{C}$ ) for the SLB formed on a nanoporous particle, as compared with  $41^\circ\text{C}$  ( $\pm 1^\circ\text{C}$ ) for the SLB formed on a solid particle;  $41^\circ\text{C}$  is the gel-to-fluid transition temperature ( $T_m$ ) of DPPC, as well as the  $T_m$  reported for unilamellar DPPC liposomes<sup>33</sup>. These data indicate that the nanoporous support results in a substantial reduction ( $6^\circ\text{C}$ ) in  $T_m$ . We reason that this melting-point suppression and the resulting enhancement in bilayer fluidity, also observed for nanoporous particle-supported DOPC bilayers (see Supplementary Fig. S3b), are consequences of unique physical constraints that exist at the interface between the bilayer and the nanoporous support. The underlying three-dimensional porosity and corresponding periodic roughness of the particle surface, which is composed of

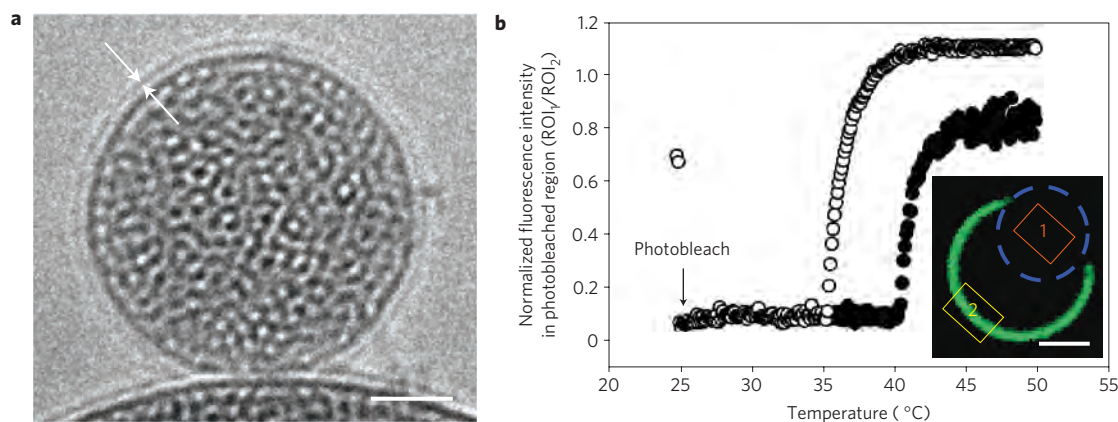


**Figure 2 | Physical and biophysical characteristics of protocells.** **a**, Cryogenic TEM image of the protocell, showing the nanoporous core and the SLB ( $\sim 4$  nm thick). Particle sizes reflect those naturally generated by the aerosol-assisted self-assembly process<sup>26</sup>; particles were separated into a narrow distribution centred around  $\sim 100$  nm for all surface-binding, internalization and delivery experiments (see Supplementary Fig. S1). Scale bar = 25 nm. **b**, Temperature-dependent FRAP of nitrobenzoxadiazole-labelled DPPC bilayers (green) supported on nanoporous (open circles) or solid (filled circles) spherical silica particles. Inset: normalized fluorescence recovery in the photobleached region (blue circle) was determined by dividing the fluorescence intensity in region of interest 1 (ROI<sub>1</sub>) by the fluorescence intensity in ROI<sub>2</sub> to account for photobleaching that occurred during the recovery period. Scale bar = 5  $\mu$ m.

nanoscopic patches of silica and water, generate localized, nanoscale gradients in adhesion and lateral tension that enhance long-range, in-plane fluidity without introducing roughness or appreciably changing the SLB's average packing density (determined by us previously by neutron reflectivity of lipid bilayers supported on planar nanoporous supports<sup>34</sup>). This conclusion is reinforced by previous experimental and theoretical studies, which found that the support suppresses all but nanoscopic, out-of-plane bilayer fluctuations<sup>35,36</sup>, as well as small-angle neutron scattering data, which indicate that the protocell SLB perfectly conforms to the underlying nanoporous silica support (see Supplementary Fig. S3a). Furthermore, on the basis of simple thermodynamic arguments, we expect particle curvature to influence bilayer fluidity only for  $R \ll (\kappa/2\varepsilon)^{1/2}$ , where  $R$  is the particle radius,  $\kappa$  is the bending modulus and  $\varepsilon$  is the adhesion energy. Given that  $\kappa = 10^{20}$  J for DOPC or DPPC and  $\varepsilon = 10^{-3}$ – $10^{-5}$  J m<sup>-2</sup>, this condition is only met when  $R \ll 100$  nm, as demonstrated by recent studies that report very slight increases in the fluidity of bilayers supported on nanowires less than 50 nm in diameter<sup>37</sup>. Overall, our data provide experimental evidence for previous theoretical predictions of the effect that nanoscale topography has on supported bilayer conformations<sup>32,38</sup>. As described below, the enhanced fluidity of nanoporous particle-supported lipid bilayers enables protocells modified with a minimal number of targeting peptides to selectively bind to and become internalized by cancer cells, whereas their enhanced stability vis-à-vis liposomes prevents drug leakage on exposure to simulated body fluids.

The schematic diagram in Fig. 3 depicts the mechanism by which targeted protocells deliver encapsulated cargo specifically to a cancer cell of interest; successive steps of binding (step 1), internalization (step 2), endosomal escape (step 3) and nuclear targeting of desired cargo(s) (step 4) are individually described below. Protocells are synthesized by fusion of liposomes to spherical, nanoporous silica cores (100–150 nm in diameter after size separation; see Figs. 1, 2a and Supplementary Fig. S1a,d) that are preloaded by simple immersion in a solution of the desired cargo. On the basis of optimization studies (see Supplementary Fig. S5) that aimed to maximize colloidal stability and cargo retention in simulated body fluids and minimize nonspecific interactions with serum proteins and non-cancerous cells, we used the following SLB composition in all surface-binding, internalization and cargo delivery experiments: DOPC (or DPPC) with 5 wt% DOPE (or DPPE), 30 wt% cholesterol and 5 wt% 18:1

(or 16:0) PEG-2000 PE (see Fig. 1 and Supplementary Fig. S4 for lipid structures). Using a heterobifunctional crosslinker with a PEG ( $n = 24$ ) spacer, SP94 peptides (H<sub>2</sub>N–SFSIIHTPLPLGGC–COOH, identified by filamentous phage display to have an affinity for unknown receptor(s) expressed by human hepatocellular carcinoma (HCC); ref. 39) were covalently conjugated to DOPE (or DPPE) moieties in the SLB (see Fig. 1) at concentrations ranging from 0.002 wt% (one peptide per particle, on average) to 5.0 wt% (2,048 peptides per particle, on average—see Supplementary Table S1). 120 nm liposomes with identical bilayer compositions were synthesized for comparative purposes.

Dissociation constants ( $K_d$ , where  $K_d$  is inversely related to affinity) were used to quantify surface binding of SP94-targeted protocells and liposomes to HCC cells (Hep3B), normal hepatocytes, endothelial cells and immune cells. All  $K_d$  values were determined at 4 °C to prevent nanocarrier internalization (see Supplementary Fig. S6 and Supplementary Methods). Figure 4a,b plot  $K_d$  values of SP94-targeted protocells and liposomes for Hep3B and hepatocytes as a function of average peptide density. Protocells with SLBs composed largely of DOPC (in a fluid state at 4 °C) have a high specific affinity ( $K_d < 1$  nM) for Hep3B, and, over the range of 6–2,048 peptides per particle, their  $K_d$  values are consistently low (0.94–0.08 nM) and relatively independent of peptide density. This trend is not observed for DOPC liposomes, where  $K_d$  values strongly depend on peptide density and are more than ten times greater than those of comparable DOPC protocells. Similarly, protocells and liposomes with bilayers composed of DPPC (in a gel-like state at 4 °C) have  $K_d$  values that are more than ten times greater than corresponding DOPC protocells and exhibit a strong dependence on peptide density. We attribute the ability of DOPC protocells to bind to HCC with high affinity at low peptide densities to recruitment of multiple SP94 peptides to the cancer cell surface. Peptide recruitment is enabled by the fluid SLB and promotes multivalent interactions between the protocell and the target cancer cell. For DPPC protocells and liposomes, multivalent binding and correspondingly high specific affinity can only be realized at high peptide densities because non-fluid bilayers impose kinetic constraints on the lateral mobility of targeting peptides. The importance of SLB fluidity in promoting the peptide recruitment process is vividly illustrated in Fig. 4c. DOPC or DPPC liposomes were fused to planar nanoporous substrates (with a three-dimensional pore structure comparable to that of the protocell

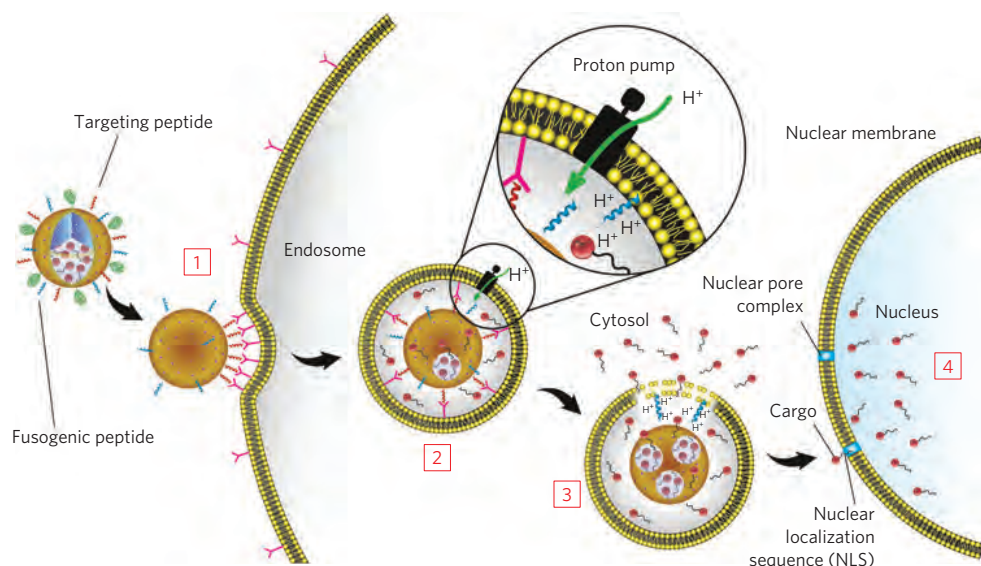


**Figure 3** | Schematic diagram depicting the successive steps of multivalent binding and internalization of targeted protocells, followed by endosomal escape and nuclear localization of protocell-encapsulated cargo. DOPC protocells (1) bind to HCC with high affinity owing to recruitment of SP94 targeting peptides (magenta) to the cell surface, (2) become internalized by receptor-mediated endocytosis and (3) release their cargo into the cytosol on endosome acidification and protonation of the H5WYG fusogenic peptide (blue). (4) Cargos modified with an NLS are transported through the nuclear pore complex and become concentrated in the nucleus.

core<sup>40,41</sup>), and the resulting SLBs were modified with a low density ( $\sim 0.015$ wt%, equivalent to  $\sim 6$  peptides/particle) of SP94 peptides. On addition of Hep3B to the supported planar bilayers, we observed rapid recruitment of SP94 to the cancer cell surface when peptides were displayed on a fluid SLB but no measurable recruitment when peptides were displayed on a non-fluid SLB. This result explains the 100-fold lower  $K_d$  value of DOPC protocells versus DPPC protocells, when both display  $\sim 6$  peptides per particle (see Fig. 4a and the following discussion).

The ability of targeting peptides, when displayed in low densities on a fluid SLB, to be recruited and multivalently bind to surface receptor(s) is crucial to enhance specific affinity, reduce nonspecific interactions and direct receptor-mediated endocytosis of nanocarriers, all of which maximize selective delivery of cargo. Concerning this point, it is important to note the influence of bilayer fluidity and stability on the peptide-density-dependent affinity of SP94-targeted protocells and liposomes for HCC (Fig. 4a) and normal hepatocytes (Fig. 4b). Non-fluid DPPC protocells and liposomes have a low affinity ( $K_d \geq 1 \mu\text{M}$ ) for hepatocytes at high SP94 densities. However, their affinity for Hep3B ( $K_d = 1\text{--}100 \text{ nM}$ ) is substantially lower than that of DOPC protocells ( $K_d < 1 \text{ nM}$ ) at all peptide densities, and their  $K_d$  values for Hep3B increase more rapidly with decreasing peptide density. DOPC protocells and liposomes have similar affinities for hepatocytes at all SP94 densities (see Fig. 4b), but the  $K_d$  values of DOPC liposomes for Hep3B are between 10 and 200 times greater than those of DOPC protocells modified with the same number of peptides (see Fig. 4a). We attribute these observations to the enhanced fluidity of nanoporous particle-supported DOPC bilayers, which enables multivalent peptide recruitment to the Hep3B surface, combined with the ability of the nanoporous core to suppress the large-scale bilayer fluctuations that, for DOPC liposomes especially, seem to act as a steric barrier to high-avidity binding. The result is that DOPC protocells modified with about six copies of the SP94 peptide have a differential  $K_d$  value (HCC/hepatocytes) of  $2.25 \times 10^4$ , which exceeds that of SP94-targeted DPPC protocells, DPPC liposomes and DOPC liposomes by more than  $10^2$ . DOPC protocells, additionally, have a  $10^4$ -fold higher affinity for HCC than for other control cells, including human endothelial cells, mononuclear cells,

B lymphocytes and T lymphocytes (see Supplementary Fig. S7). Also, the  $K_d$  value of DOPC protocells for Hep3B is 200 times lower than that of free SP94 for Hep3B and nearly 50,000 times lower than that of unmodified protocells for Hep3B (see Supplementary Fig. S7). If sub-nanomolar affinity is undesirable (results in reduced tumour penetration, for example), the  $K_d$  values of SP94-targeted protocells can be precisely modulated by incorporating various amounts of fluid and non-fluid lipids into the SLB (see Supplementary Fig. S8).

DOPC protocells are uniquely able to target HCC at low peptide densities, and their dramatic differential affinity for HCC translates into selective internalization when the experimental temperature is raised from 4 to 37 °C. DOPC protocells modified with a low density of SP94 peptides ( $\sim 0.015$  wt%) are efficiently endocytosed by Hep3B but not by hepatocytes, as demonstrated by the representative confocal fluorescence microscopy images shown in Fig. 4d,e; see also Supplementary Table S2, which lists average numbers of SP94-targeted protocells and liposomes internalized by Hep3B and hepatocytes. The efficacy with which targeted protocells are internalized by Hep3B depends largely on binding affinity, which can be modulated by changing bilayer fluidity and ligand density. However, it also depends on nanocarrier size (see Supplementary Fig. S9), with 50 nm protocells being most efficiently internalized ( $\sim 1,800$  particles/cell). This result provides evidence that internalization occurs through an endocytotic pathway, given that membrane wrapping occurs most efficiently for particles 30–60 nm in diameter<sup>11</sup>. Despite this observation, we use protocells 100–150 nm in diameter for targeted delivery, because the increased cargo capacity, which we measure to be proportional to the cube of the particle radius, more than compensates for the slightly reduced internalization efficiency.

To demonstrate that high-affinity surface binding followed by receptor-mediated endocytosis enables targeted delivery of multicomponent cargos, we loaded four fluorescently labelled surrogates, similar in size and charge to common therapeutic and diagnostic agents, within the protocell core. Figure 5a shows simultaneous encapsulation of a low-molecular-weight drug mimic (calcein), a small interfering RNA (siRNA) mimic (double-stranded DNA, dsDNA), a protein toxin mimic (red fluorescent protein,

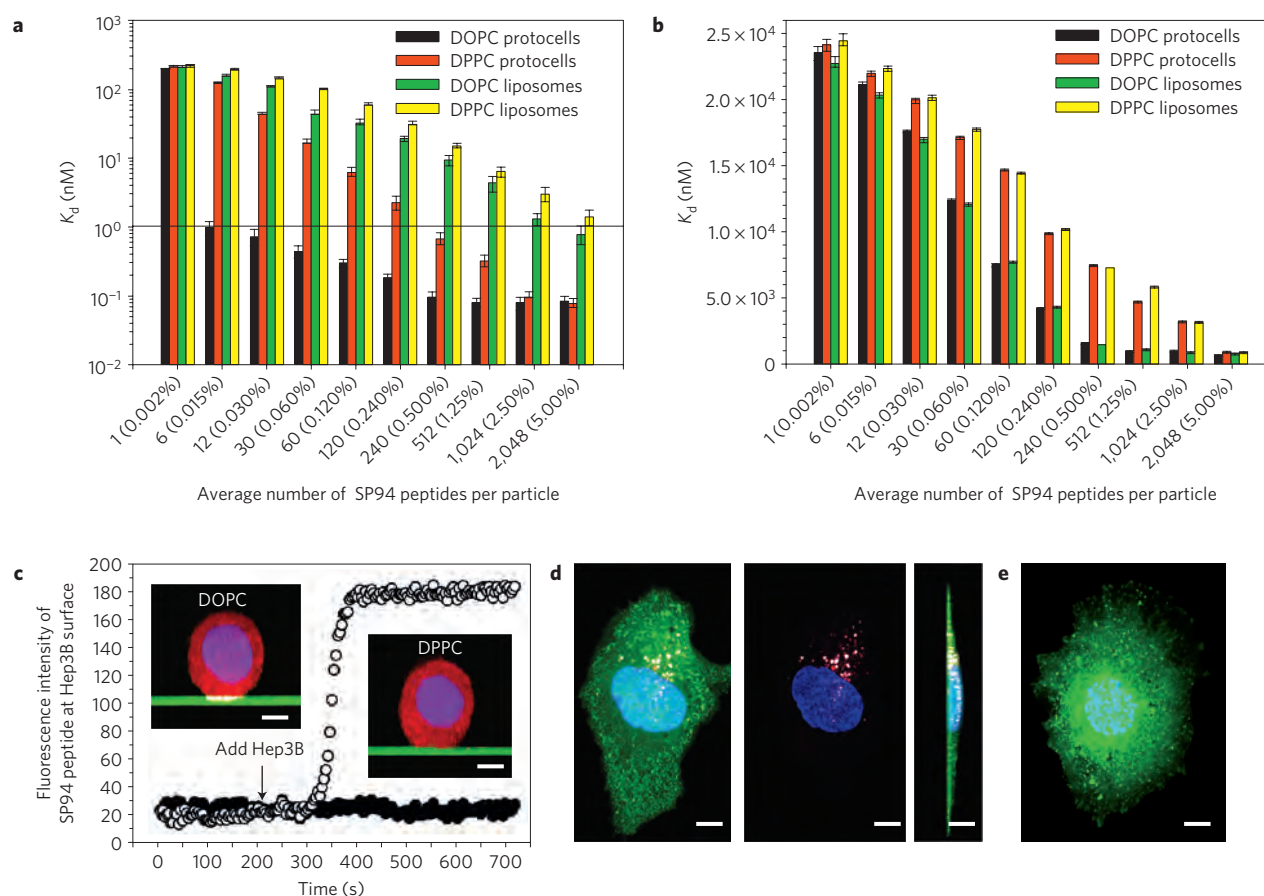


**Figure 4 | Selective binding and internalization characteristics of SP94-targeted protocells.** **a, b**, Dissociation constants ( $K_d$ ) of SP94-targeted protocells and liposomes for Hep3B (**a**) and hepatocytes (**b**) as a function of the average number of SP94 peptides per particle (average SP94 wt% is in parentheses). All surface-binding experiments were conducted at 4 °C to prevent internalization of targeted protocells and liposomes. All error bars in **a** and **b** represent 95% confidence intervals ( $1.96\sigma$ ) for  $n = 5$ . **c**, Recruitment of Alexa Fluor 647-labelled SP94 peptides (white) to the surface of a Hep3B cell when peptides are displayed on a nitrobenzoxadiazole-labelled SLB (green) composed of DOPC (open circles) or DPPC (closed circles). These data were collected at 4 °C to replicate the conditions used to determine  $K_d$  values in **a** and **b**. Hep3B cells were labelled with CellTracker Red CMTPX (red) and Hoechst 33342 (blue). Inset scale bars = 5  $\mu\text{m}$ . **d, e**, Confocal fluorescence microscopy images of Hep3B (**d**) and hepatocytes (**e**) incubated with SP94-targeted protocells for 1 hour at 37 °C. Protocells were prepared with Texas Red-labelled DHPE (red) and Alexa Fluor 647-labelled nanoporous cores (white); cells were stained with CellTracker Green CMFDA (green) and Hoechst 33342 (blue). Cells shown in **d** and **e** are representative of the entire cell population (see Supplementary Table S2 for population-based internalization data); single cells were selected to enable three-dimensional imaging. Plan (left and centre images) and cross-sectional (right image) views of the three-dimensional projection are shown for **d**, whereas the plan view alone is shown for **e**. For **d**, the merged plan view (left) is shown without the green channel (centre) to enable better visualization of lipid (red) and silica (white) moieties. It is important to note that plan views of collapsed projections superimpose all slices in the  $z$  direction, giving the misleading appearance of protocells in the nucleus of **d**; this is not the case, however, as is evident in an orthogonal view of the projection (image not shown). All scale bars = 10  $\mu\text{m}$ .

RFP) and a model nanoparticle (water-soluble CdSe/ZnS quantum dots), all within a fluorescently labelled porous silica particle that is completely encased in a fluorescently labelled DOPC bilayer; a protocell 10  $\mu\text{m}$  in diameter was employed in this experiment to enable optical imaging. The confocal slice ( $z = 5 \mu\text{m}$ ) demonstrates that the multiple cargos are uniformly distributed throughout the silica core and that the SLB is intact and coherent.

As illustrated schematically in Fig. 3 and confirmed by hyperspectral confocal fluorescence microscopy (Fig. 5b–d), delivery of encapsulated cargo to HCC using SP94-targeted DOPC protocells is achieved by the following successive steps. (1) Multivalent binding of SP94 to HCC surface receptor(s) initiates receptor-mediated endocytosis, an internalization pathway that helps to circumvent MDR (ref. 42). Peptide recruitment to the cell surface promotes the multivalent effects that enhance specificity. (2) As shown by the appearance of punctuate regions containing co-localized lipid, silica and cargo in Fig. 5b, protocells are rapidly endocytosed (half-life  $t_{1/2} = 15 \text{ min}$ ) by Hep3B cells and reach a

satürating intracellular concentration (~500 protocells per Hep3B cell; see Supplementary Table S2) within an hour. Given that the SP94 peptide directs protocells to lysosomes on endocytosis by Hep3B (see Supplementary Fig. S10), we further modified the SLB with 0.500 wt% of a histidine-rich fusogenic peptide (H5WYG,  $\text{H}_2\text{N}-\text{GLFHAIAHFHGGWHGLIHGWYGGGC}-\text{COOH}$ ; ref. 43), which, in addition to preventing degradation of sensitive cargos in endolysosomes, promotes endosomal escape of protocells and cytosolic dispersion of encapsulated cargos (see Supplementary Fig. S11). (3) Endosome acidification destabilizes the SLB (see Supplementary Fig. S12), enabling encapsulated cargo to diffuse out of the nanoporous core. Additionally, protonation of imidazole moieties ( $pK_a = 6.0$ ) in the fusogenic peptide initiates osmotic swelling and membrane destabilization of endosomes through the ‘proton sponge’ mechanism<sup>44</sup>. As shown in Fig. 5c, these events enable the four surrogate cargos, along with lipid and silica moieties of the protocell, to become distributed throughout the cytosol within 4 h. (4) Cargos modified with a nuclear localization

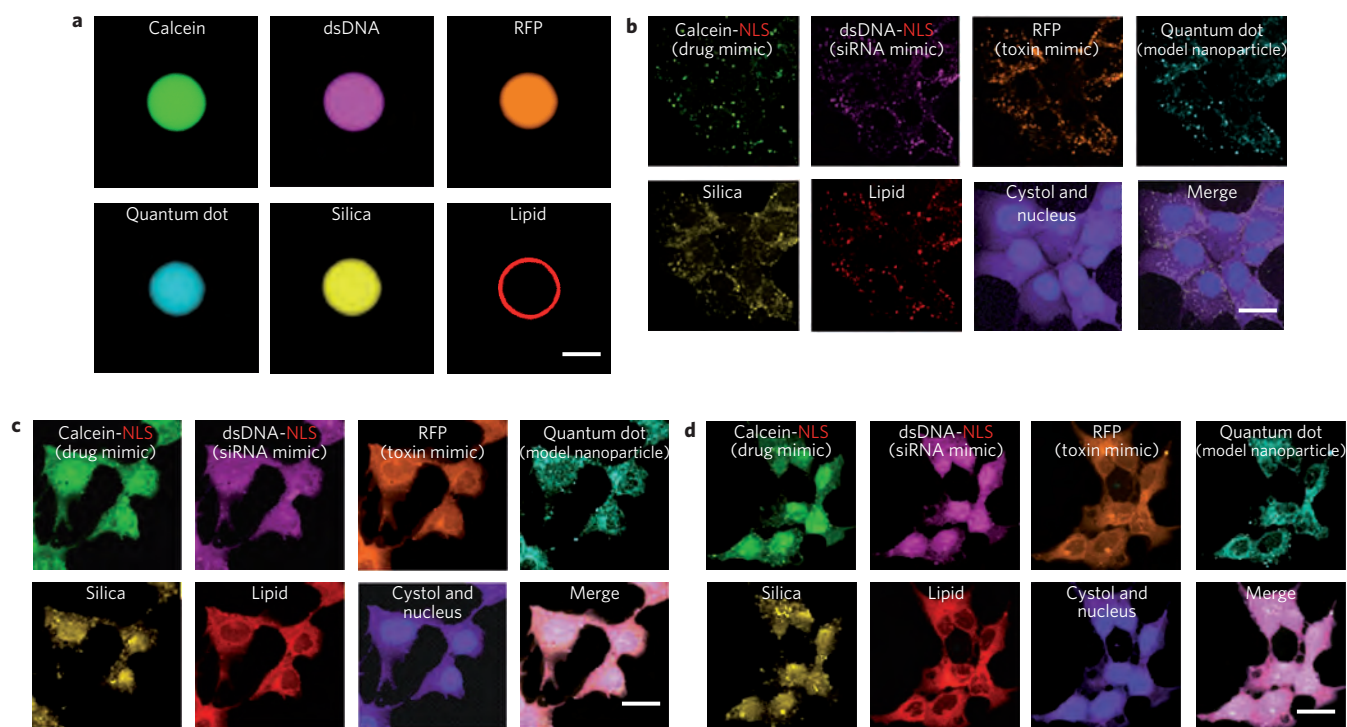


**Figure 5 | Targeted delivery of multicomponent cargos to the cytosol and nuclei of HCC cells. a–d,** Alexa Fluor 532-labelled nanoporous silica cores (yellow) were loaded with a multicomponent mixture of four surrogate cargos: calcein (green), an Alexa Fluor 647-labelled dsDNA oligonucleotide (magenta), RFP (orange) and CdSe/ZnS quantum dots (teal). Cargos were sealed in the cores by fusion of Texas Red-labelled DOPC liposomes (red) that contained 30 wt% cholesterol and 5 wt% PEG-2000 PE, and the resulting SLBs were modified with 0.015 wt% SP94 and 0.500 wt% H5WYG. Protocells were incubated with Hep3B cells (labelled with CellTracker Violet BMQC and Hoechst 33342) for 15 min, 4 h or 12 h (respectively) at 37 °C to collect the images shown in **b–d**. **a**, Hyperspectral confocal fluorescence microscopy slice ( $z \approx 5 \mu\text{m}$ ) of a 10  $\mu\text{m}$  protocell, demonstrating uniform loading of the nanoporous silica core and complete encapsulation of the core and cargos within the SLB. Particles 100 times larger than those used for all surface-binding, internalization and delivery studies were used in this experiment to enable optical imaging and have a  $2.5 \times 10^5$  times higher capacity for the multicomponent mixture than protocells (100–150 nm in diameter) used to collect the images shown in **b–d**. Scale bar = 5  $\mu\text{m}$ . **b–d**, Hyperspectral confocal fluorescence microscopy was employed to individually track the lipid and silica moieties of DOPC protocells (100–150 nm multimodal core), as well as the four surrogate cargos within the cytosol (purple) and nuclei (blue) of Hep3B cells as a function of time. **b**, Within 15 min of exposing Hep3B to protocells loaded with the multicomponent mixture, the lipid, silica and cargo moieties have a punctate appearance, indicating that protocells are localized within endosomes. **c**, Within 4 h, the H5WYG peptide promotes endosomal escape, thereby releasing the lipid, silica and cargos into the cytosol of the Hep3B cells. **d**, Within 12 h, calcein and the dsDNA oligonucleotide, both of which are modified with an NLS, become concentrated in the nucleus, whereas the RFP and quantum dots (not modified with an NLS) remain largely localized in the cytosol. Protocells used to collect the images shown in **b–d** have a high capacity for the multicomponent mixture:  $10^{10}$  protocells encapsulate 425  $\mu\text{mol}$  of calcein, 7.6  $\mu\text{mol}$  of the dsDNA oligonucleotide, 945 nmol of RFP, and  $1.98 \times 10^{13}$  quantum dots. Scale bars = 20  $\mu\text{m}$ .

sequence (NLS; ref. 45) become concentrated in the nucleus, because the NLS promotes transport through the nuclear pore complex. Figure 5d demonstrates that NLS-modified calcein and dsDNA become localized in the nuclei of Hep3B cells within 12 h, whereas RFP and quantum dots (not modified with the NLS) remain concentrated in the cytosol.

We have used the above sequence of events to deliver high payloads of various cytotoxic agents to HCC, including drugs and drug cocktails, siRNA cocktails (see Supplementary Figs S13 and S14) and protein toxins (see Supplementary Figs S15 and S16) without affecting the viability of hepatocytes and other control cells. Figure 6 compares the cargo capacity, time-dependent release characteristics and selective cytotoxicity of SP94-targeted protocells and liposomes loaded with the chemotherapeutic drug doxorubicin (DOX). Protocells, owing to the high surface area and porosity of their nanoporous cores, have a 1,000 times higher capacity for DOX than similarly sized liposomes (loaded through an ammonium phosphate gradient-based approach<sup>46</sup>) and can be engineered to release nearly 90% of their encapsulated DOX in a bioactive form on endocytosis by HCC (see ‘Effective capacity’ in Fig. 6a, left axis). Additionally, DOPC protocells exhibit long-term stability when

maintained in a simulated body fluid (pH 7.4) at 37 °C, whereas DOPC liposomes leak 90% of their encapsulated DOX within 72 h and have a release profile comparable to that of the nanoporous core with no SLB. Thus, the fluid lipids that enable selective targeting at low peptide densities cannot be used in liposomal drug formulations, because premature release of encapsulated cargo results in undesired toxicity to non-cancerous cells. Stable formulations of liposomal drugs require the use of fully saturated, high- $T_m$  lipids (for example 1,2-distearoyl-*sn*-glycero-3-phosphocholine (DSPC),  $T_m = 55 \text{ }^\circ\text{C}$ ) and high concentrations of cholesterol, which act cooperatively to increase the lipid packing density and limit diffusion of the drug across the bilayer<sup>47</sup>. Even the stability of ‘gold standard’ liposomal DOX (for example DSPC with 30 wt% cholesterol and 5 wt% PEG) remains limited, however, as up to 25% of the drug is released within 72 h when exposed to a simulated body fluid at 37 °C (see ‘DSPC liposomes’ in Fig. 6b).

Exposing protocells to a pH 5.0 buffer, which simulates the endosomal environment and destabilizes the SLB (see Supplementary Fig. S12), promotes rapid release of drugs loaded within the nanoporous core; DOPC protocells release 99% of their encapsulated DOX within 12 h (see Fig. 6c). DSPC and DOPC

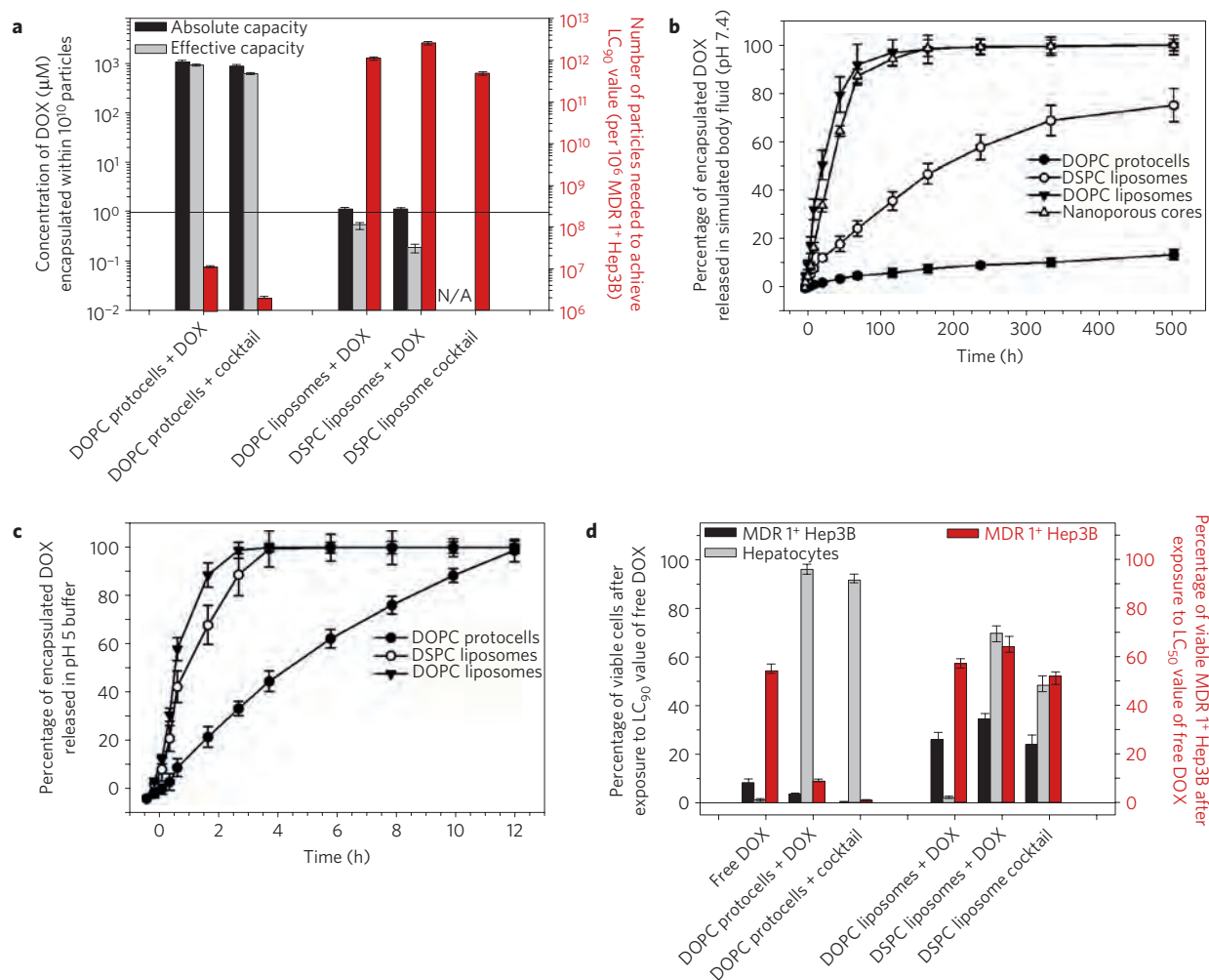


**Figure 6 | Cargo capacity, time-dependent release profiles and concentration-dependent cytotoxicity of SP94-targeted protocells and liposomes that encapsulate chemotherapeutic drugs.** **a**, Cargo capacity and cytotoxicity of protocells and liposomes loaded with DOX. Left axis: The absolute and effective capacities of DOPC protocells, DOPC liposomes and DSPC liposomes for DOX. Absolute capacity is defined as the concentration of DOX that can be physically encapsulated within  $10^{10}$  particles, whereas effective capacity is the concentration of DOX that is released on endocytosis by Hep3B in a form capable of intercalating nuclear DNA. DOPC protocells, when loaded with a cocktail of DOX, 5-fluorouracil (5-FU) and cisplatin, retain their high absolute and effective capacities. The liposome cocktail is composed of equal volumes of DOX-loaded, 5-FU-loaded and cisplatin-loaded DSPC liposomes. DSPC liposomes that encapsulate 5-FU have an absolute capacity of  $765 \text{ nM}$  (per  $10^{10}$  particles) and were prepared using the reverse-phase evaporation method described in ref. 52. DSPC liposomes that encapsulate cisplatin have an absolute capacity of  $980 \text{ nM}$  (per  $10^{10}$  particles) and were prepared using the technique described in ref. 53. Right axis: The number of DOX-loaded protocells or liposomes that must be added to  $10^6$  MDR1<sup>+</sup> Hep3B cells to kill 90% of the cells in the population ( $\text{LC}_{90}$ ) within 24 h. **b**, The time-dependent release of DOX from DOPC protocells, DSPC liposomes, DOPC liposomes and nanoporous silica cores when exposed to a simulated body fluid (pH 7.4) at  $37^\circ\text{C}$  for 21 days. **c**, The time-dependent release of DOX from DOPC protocells, DSPC liposomes and DOPC liposomes when exposed to a pH 5 citric acid buffer at  $37^\circ\text{C}$  for 12 h. Acidic conditions, which mimic those of the endosome, destabilize the SLB and promote release of DOX from the protocell's nanoporous core. **d**, Left axis: The number of MDR1<sup>+</sup> Hep3B and hepatocytes that remain viable after exposure to  $9.6 \mu\text{M}$  of free DOX, protocell-encapsulated DOX or liposomal DOX for 24 h at  $37^\circ\text{C}$ .  $9.6 \mu\text{M}$  is the  $\text{LC}_{90}$  value of free DOX when exposed to Hep3B with induced MDR (MDR1<sup>+</sup> phenotype) and was, therefore, selected as the standardized drug concentration. Cells were exposed to drugs and drug-loaded nanocarriers for 24 h because the typical doubling time of HCC is 24–36 h. Right axis: The number of MDR1<sup>+</sup> Hep3B that remain viable after exposure to  $2.4 \mu\text{M}$  free DOX, protocell-encapsulated DOX or liposomal DOX for 24 h at  $37^\circ\text{C}$ ;  $2.4 \mu\text{M}$  is the  $\text{LC}_{50}$  value of free DOX. Sytox Green nucleic acid stain and Alexa Fluor 647-labelled annexin V were used to distinguish viable (double-negative) from non-viable (single- or double-positive) cells. All error bars represent 95% confidence intervals ( $1.96\sigma$ ) for  $n = 3$ .

liposomes release nearly all of their encapsulated DOX on exposure to a pH 5.0 buffer for 4 h (see Fig. 6c). Differences in absolute cargo capacities must be taken into account, however, to accurately compare the drug delivery capabilities of targeted protocells and liposomes. DOPC protocells release  $\sim 50\%$  of their encapsulated DOX within 4 h, which corresponds to a drug concentration of nearly  $500 \mu\text{M}$  when the protocell concentration is maintained at  $10^{10}$  particles  $\text{ml}^{-1}$ . In comparison,  $10^{10}$  liposomes release only  $\sim 1 \mu\text{M}$  of DOX in the same period of time. It is important to

note that the DSPC liposomes referred to in Fig. 6 have a similar capacity for DOX ( $\sim 1.1 \mu\text{M}$  per  $10^{10}$  particles), which corresponds to a drug:lipid ratio of 0.113:1) to other PEGylated liposomal DOX formulations, including Doxil (drug:lipid ratio of 0.125:1; ref. 47).

The unique properties of drug-loaded DOPC protocells modified with a minimal number of targeting peptides solve the conundrum of simultaneously achieving high targeting specificity, high cytotoxicity to the target cell, and low collateral damage to non-cancerous cells. Figure 6a (right axis) plots the number

of DOX-loaded DOPC protocells, DSPC liposomes and DOPC liposomes needed to kill 90% of Hep3B ( $LC_{90}$ ) with an induced MDR1 phenotype. We find that  $10^5$  fewer DOX-loaded protocells are necessary to achieve this  $LC_{90}$  value when compared with DOX-loaded DSPC or DOPC liposomes. Figure 6d (left axis) plots the percentage of Hep3B and hepatocytes that remain viable after exposure to either free DOX or to DOX encapsulated within DOPC protocells, DSPC liposomes or DOPC liposomes for 24 h at 37 °C; here the total DOX concentration was normalized to 9.6  $\mu$ M, which is the concentration of free DOX necessary to kill 90% of MDR1<sup>+</sup> Hep3B within 24 h. We observe that DOX-loaded DOPC protocells maintain greater than 90% hepatocyte viability, while killing nearly 97% of MDR1<sup>+</sup> Hep3B. In comparison, DOX-loaded DSPC and DOPC liposomes are less efficient at killing HCC and cause significant cytotoxicity to non-cancerous cells. Figure 6d (right axis) shows the number of MDR1<sup>+</sup> Hep3B that remain viable after incubation with a lower concentration (2.3  $\mu$ M, the  $LC_{50}$  value of free DOX) of free DOX, DOX-loaded protocells or DOX-loaded liposomes. These data are included to clearly demonstrate the enhanced killing efficacy of DOX-loaded protocells when compared with both free DOX and DOX-loaded liposomes, an observation that is further supported by the fact that DOX-loaded protocells decrease the  $LC_{90}$  value of free DOX (9.6  $\mu$ M) to  $\sim$ 145 nM. We attribute the striking differences shown in Fig. 6a (right axis) and 6d to the 1,000 times higher capacity (Fig. 6a, left axis), the enhanced binding affinity (Fig. 4a) and the greater long-term stability (Fig. 6b) of DOPC protocells. These factors synergistically combine to provide dramatic improvements in selective cytotoxicity of cancer, while limiting undesired toxicity to normal hepatocytes. Protocells can, furthermore, be easily loaded with multicomponent cargos by simply soaking the nanoporous core in a solution of the desired cargos before fusion of the SLB. Figure 6a (right axis) and 6d show that, when loaded with a cocktail of DOX, 5-fluorouracil and cisplatin (a chemotherapeutic drug cocktail known to be particularly effective against drug-resistant HCC; ref. 48), as little as one SP94-targeted DOPC protocell is sufficient to kill a Hep3B cell with an induced MDR1 phenotype while maintaining more than 90% hepatocyte viability. Similar results cannot be achieved using DOPC and DSPC liposomes, because liposomes cannot be loaded with drug cocktails using strategies based on transmembrane pH gradients. A cocktail of DSPC liposomes that individually encapsulate DOX, 5-FU or cisplatin was employed as a control but failed to substantially improve on the selective cytotoxicity of DOX-loaded DSPC liposomes (see Fig. 6a,d).

We have demonstrated that targeted protocells possess the high specificity, enhanced cargo capacity and long-term stability necessary to deliver a variety of chemically disparate therapeutic and diagnostic agents to cancer cells with minimal nonspecific binding and toxicity to normal cells. We have, furthermore, shown that the nanoporous core can be adapted to release encapsulated cargo within 24 h or over the course of several weeks (see Supplementary Fig. S2), and that the SLB can be modified with a variety of ligands, including peptides, antibodies and glycoproteins, to promote specific affinity for a target cell (see section 2 in Supplementary Figures and Legends).

So far, no other nanoparticle-based delivery vehicle has been reported that possesses all of these attributes, making protocells the first example of a nanocarrier that simultaneously addresses the complex requirements of targeted, multicomponent delivery. Perhaps the most striking feature of protocells is their ability to deliver high concentrations of diverse cargos and 'cocktails' of chemically disparate components. For example, Supplementary Figs S13 and S14 report preliminary data regarding the killing efficacy of SP94-targeted protocells loaded with an siRNA cocktail that silences expression of epidermal growth factor receptor, vascular endothelial growth factor receptor-2 and platelet-derived growth

factor receptor- $\alpha$ . Protocells encapsulate 1,000 times more siRNA than similarly sized liposomes with the same bilayer composition and, when targeted with the SP94 peptide, induce apoptosis in 50% of Hep3B within 36 h without affecting the viability of hepatocytes. Another distinctive characteristic of protocells is that the enhanced fluidity and stability of the SLB support multivalent peptide recruitment to surface receptors expressed by the target cell, which suggests that displaying two or more types of ligand on the protocell surface might enable complex binding interactions. We expect, therefore, that modifying the protocell SLB with ligand(s) that bind to surface receptor(s) uniquely or overexpressed by the target cell along with a ligand that promotes internalization (for example the octaarginine peptide, which stimulates macropinocytosis<sup>49</sup>) would enable both selective targeting and intracellular delivery for cancers where cell-specific receptors are not normally endocytosed.

## Methods

Nanoporous silica particles were synthesized and characterized as described previously<sup>26,50</sup> and as detailed in Supplementary Fig. S1 and the Supplementary Methods section. Particles larger than  $\sim$ 150-nm in diameter were removed by differential centrifugation or size-exclusion chromatography (see Supplementary Fig. S1a,d). Protocells were formed by fusing  $\sim$ 120 nm liposomes to the nanoporous core as reported previously<sup>23–25</sup>, and the composition of the SLB was optimized to reduce nonspecific binding associated with cationic and, to a lesser extent, anionic lipids<sup>51</sup> (see Supplementary Fig. S5). Zwitterionic lipids (DOPC or DPPC) with 5 wt% PE (DOPE or DPPE, respectively), 5 wt% PEG-2000 PE (18:0 or 16:0, respectively) and 30 wt% cholesterol were used in all further studies; PEGylated lipids were incorporated into the liposomes used for fusion and are, therefore, expected to be present on both the inner and outer leaflets of the SLB. The size of the nanoporous core was also optimized to attain a balance between achievable cargo capacity and the rate of protocell internalization (see Supplementary Fig. S9); nanoparticles 100–150 nm in diameter were employed in the delivery of drugs, drug cocktails, siRNA cocktails and protein toxins. The nanoporous cores were soaked in a 10 mM solution of cargo(s) for 1–12 h before liposome fusion; individual components of the surrogate cargo mixture (Fig. 5) and the drug cocktail (Fig. 6) were loaded into nanoporous cores simultaneously (as opposed to sequentially). The rates of cargo release were optimized by incorporating various percentages of AEPTMS, an amine-containing silane, into the sol used to form nanoporous cores (see Supplementary Fig. S2). Particles containing 15 wt% AEPTMS were used to deliver drugs and drug cocktails (Fig. 6), whereas particles containing 20 wt% AEPTMS were used to deliver the multicomponent mixture (Fig. 5), the siRNA cocktail (Supplementary Fig. S13 and 14) and diphtheria toxin A-chain (Supplementary Figs S15 and S16).

Received 17 May 2010; accepted 24 February 2011;  
published online 17 April 2011; corrected online 10 May 2011

## References

- Peer, D. *et al.* Nanocarriers as an emerging platform for cancer therapy. *Nature Nanotech.* **2**, 751–760 (2007).
- Wagner, V., Dullaart, A., Bock, A.-K. & Zwick, A. The emerging nanomedicine landscape. *Nature Biotechnol.* **24**, 1211–1217 (2006).
- Nel, A. E. *et al.* Understanding biophysicochemical interactions at the nano–bio interface. *Nature Mater.* **8**, 543–557 (2009).
- Ferrari, M. Cancer nanotechnology: Opportunities and challenges. *Nature Rev. Cancer* **5**, 161–171 (2005).
- Maeda, H., Wu, J., Sawa, T., Matsumura, Y. & Hori, K. Tumor vascular permeability and the EPR effect in macromolecular therapeutics: A review. *J. Control. Release* **65**, 271–284 (2000).
- Matsumura, Y. & Maeda, H. A new concept for macromolecular therapeutics in cancer chemotherapy: Mechanism of tumoritropic accumulation of proteins and the antitumor agent SMANCS. *Cancer Res.* **46**, 6387–6392 (1986).
- Gottesman, M. M., Fojo, T. & Bates, S. E. Multidrug resistance in cancer: Role of ATP-dependent transporters. *Nature Rev. Cancer* **2**, 48–58 (2002).
- Kohlschütter, J., Michelfelder, S. & Trepel, M. Drug delivery in acute myeloid leukemia. *Expert Opin. Drug Deliv.* **5**, 653–663 (2008).
- Torchilin, V. P. Recent advances with liposomes as pharmaceutical carriers. *Nature Rev. Drug Discov.* **4**, 145–160 (2005).
- Rai, P. *et al.* Statistical pattern matching facilitates the design of polyvalent inhibitors of anthrax and cholera toxins. *Nature Biotechnol.* **24**, 582–586 (2006).
- Jiang, W., Kim, B. Y. S., Rutka, J. T. & Chan, W. C. W. Nanoparticle-mediated cellular response is size-dependent. *Nature Nanotech.* **3**, 145–150 (2008).
- Pastan, I., Hassan, R., FitzGerald, D. J. & Kreitman, R. J. Immunotoxin therapy of cancer. *Nature Rev. Cancer* **6**, 559–565 (2006).
- Ferrari, M. Nanogeometry: Beyond drug delivery. *Nature Nanotech.* **3**, 131–132 (2008).

14. Giri, S., Trewny, B. G., Stellmaker, M. P. & Lin, V. S. Y. Stimuli-responsive controlled-release delivery system based on mesoporous silica nanorods capped with magnetic nanoparticles. *Angew. Chem. Int. Ed.* **44**, 5038–5044 (2005).
15. Lai, C.-Y. *et al.* A mesoporous silica nanosphere-based carrier system with chemically removable CdS nanoparticle caps for stimuli-responsive controlled release of neurotransmitters and drug molecules. *J. Am. Chem. Soc.* **125**, 4451–4459 (2003).
16. Liong, M. *et al.* Multifunctional inorganic nanoparticles for imaging, targeting, and drug delivery. *ACS Nano* **2**, 889–896 (2008).
17. Nguyen, T. D. *et al.* A reversible molecular valve. *Proc. Natl Acad. Sci. USA* **102**, 10029–10034 (2005).
18. Patel, K. *et al.* Enzyme-responsive snap-top covered silica nanocontainers. *J. Am. Chem. Soc.* **130**, 2382–2383 (2008).
19. Vallet-Regí, M., Balas, F. & Arcos, D. Mesoporous materials for drug delivery. *Angew. Chem. Int. Ed.* **46**, 7548–7558 (2007).
20. Davis, M. E., Chen, Z. & Shin, D. M. Nanoparticle therapeutics: An emerging treatment modality for cancer. *Nature Rev. Drug Discov.* **7**, 771–782 (2008).
21. Gordon, A. N. *et al.* Recurrent epithelial ovarian carcinoma: A randomized phase III study of pegylated liposomal doxorubicin versus topotecan. *J. Clin. Oncol.* **19**, 3312–3322 (2001).
22. Peer, D., Zhu, P., Carman, C. V., Lieberman, J. & Shimaoka, M. Selective gene silencing in activated leukocytes by targeting siRNAs to the integrin lymphocyte function-associated antigen-1. *Proc. Natl Acad. Sci. USA* **104**, 4095–4100 (2007).
23. Liu, J. W., Jiang, X. M., Ashley, C. & Brinker, C. J. Electrostatically mediated liposome fusion and lipid exchange with a nanoparticle-supported bilayer for control of surface charge, drug containment, and delivery. *J. Am. Chem. Soc.* **131**, 7567–7569 (2009).
24. Liu, J. W., Stace-Naughton, A. & Brinker, C. J. Silica nanoparticle supported lipid bilayers for gene delivery. *Chem. Commun.* 5100–5102 (2009).
25. Liu, J. W., Stace-Naughton, A., Jiang, X. M. & Brinker, C. J. Porous nanoparticle supported lipid bilayers (protocells) as delivery vehicles. *J. Am. Chem. Soc.* **131**, 1354–1355 (2009).
26. Lu, Y. F. *et al.* Aerosol-assisted self-assembly of mesostructured spherical nanoparticles. *Nature* **398**, 223–226 (1999).
27. Evans, E. Entropy-driven tension in vesicle membranes and unbinding of adherent vesicles. *Langmuir* **7**, 1900–1908 (1991).
28. Komura, S., Shimokawa, N. & Andelman, D. Tension-induced morphological transition in mixed lipid bilayers. *Langmuir* **22**, 6771–6774 (2006).
29. Lipowsky, R. The conformation of membranes. *Nature* **349**, 475–481 (1991).
30. Mutz, M. & Helfrich, W. Unbinding transition of a biological model membrane. *Phys. Rev. Lett.* **62**, 2881–2884 (1989).
31. Netz, R. R. & Lipowsky, R. Stacks of fluid membranes under pressure and tension. *Europhys. Lett.* **29**, 345–350 (1995).
32. Swain, P. S. & Andelman, D. Supported membranes on chemically structured and rough surfaces. *Phys. Rev. E* **63**, 051911 (2001).
33. Bothun, G. D., Knutson, B. L., Strobel, H. J. & Nokes, S. E. Liposome fluidization and melting point depression by pressurized CO<sub>2</sub> determined by fluorescence anisotropy. *Langmuir* **21**, 530–536 (2004).
34. Doshi, D. A. *et al.* Neutron reflectivity study of lipid membranes assembled on ordered nanocomposite and nanoporous silica thin films. *Langmuir* **21**, 2865–2870 (2005).
35. Daillant, J. *et al.* Structure and fluctuations of a single floating lipid bilayer. *Proc. Natl Acad. Sci. USA* **102**, 11639–11644 (2005).
36. Malaquin, L., Charitat, T. & Daillant, J. Supported bilayers: Combined specular and diffuse X-ray scattering. *Eur. Phys. J. E* **31**, 285–301 (2010).
37. Huang, S.-C. J. *et al.* Formation, stability, and mobility of one-dimensional lipid bilayers on polysilicon nanowires. *Nano Lett.* **7**, 3355–3359 (2007).
38. Swain, P. S. & Andelman, D. The influence of substrate structure on membrane adhesion. *Langmuir* **15**, 8902–8914 (1999).
39. Lo, A., Lin, C. T. & Wu, H. C. Hepatocellular carcinoma cell-specific peptide ligand for targeted drug delivery. *Mol. Cancer Therapeut.* **7**, 579–589 (2008).
40. Chen, Z. *et al.* DNA translocation through an array of kinked nanopores. *Nature Mater.* **9**, 667–675 (2010).
41. Lu, Y. F. *et al.* Continuous formation of supported cubic and hexagonal mesoporous films by sol gel dip-coating. *Nature* **389**, 364–368 (1997).
42. Goren, D. *et al.* Nuclear delivery of doxorubicin via folate-targeted liposomes with bypass of multidrug-resistance efflux pump. *Clin. Cancer Res.* **6**, 1949–1957 (2000).
43. Midoux, P., Kichler, A., Boutin, V., Maurizot, J.-C. & Monsigny, M. Membrane permeabilization and efficient gene transfer by a peptide containing several histidines. *Bioconj. Chem.* **9**, 260–267 (1998).
44. Behr, J. P. The proton sponge: A trick to enter cells the viruses did not exploit. *CHIMIA Int. J. Chem.* **51**, 34–36 (1997).
45. Subramanian, A., Ranganathan, P. & Diamond, S. L. Nuclear targeting peptide scaffolds for lipofection of nondividing mammalian cells. *Nature Biotechnol.* **17**, 873–877 (1999).
46. Fritze, A., Hens, F., Kimpfler, A., Schubert, R. & Peschka-Süss, R. Remote loading of doxorubicin into liposomes driven by a transmembrane phosphate gradient. *Biochim. Biophys. Acta Biomembr.* **1758**, 1633–1640 (2006).
47. Drummond, D. C., Meyer, O., Hong, K., Kirpotin, D. B. & Papahadjopoulos, D. Optimizing liposomes for delivery of chemotherapeutic agents to solid tumors. *Pharmacol. Rev.* **51**, 691–744 (1999).
48. Lee, J. O. *et al.* Combination chemotherapy with capecitabine and cisplatin for patients with metastatic hepatocellular carcinoma. *Ann. Oncol.* **20**, 1402–1407 (2009).
49. Khalil, I. A., Kogure, K. & Futaki, S. High density of octaarginine stimulates macropinocytosis leading to efficient intracellular trafficking for gene expression. *J. Biol. Chem.* **281**, 3544–3551 (2006).
50. Carroll, N. J., Pylypenko, S., Atanassov, P. B. & Petsev, D. N. Microparticles with bimodal nanoporosity derived by microemulsion templating. *Langmuir* **25**, 13540–13544 (2009).
51. Xia, T. *et al.* Comparison of the mechanism of toxicity of zinc oxide and cerium oxide nanoparticles based on dissolution and oxidative stress properties. *ACS Nano* **2**, 2121–2134 (2008).
52. Elorza, B., Elorza, M. A., Frutos, G. & Chantres, J. R. Characterization of 5-fluorouracil loaded liposomes prepared by reverse-phase evaporation or freezing–thawing extrusion methods: Study of drug release. *Biochim. et Biophys. Acta* **1153**, 135–142 (1993).
53. Peleg-Shulman, T., Gibson, D., Cohen, R., Abra, R. & Barenholz, Y. Characterization of sterically stabilized cisplatin liposomes by nuclear magnetic resonance. *Biochim. Biophys. Acta* **1510**, 278–291 (2001).

## Acknowledgements

This work was supported by the NIH/Roadmap for Medical Research under grant PHS 2 PN2 EY016570B; NCI Cancer Nanotechnology Platform Partnership grant 1U01CA151792-01; the Air Force Office of Scientific Research grant FA 9550-07-1-0054/9550-10-1-0054; the US Department of Energy, Office of Basic Energy Sciences, Division of Materials Sciences and Engineering; the Sandia National Laboratories' Laboratory Directed Research and Development (LDRD) programme; the President Harry S. Truman Fellowship in National Security Science and Engineering at Sandia National Laboratories (C.E.A.); the UCLA Center for Nanobiology and Predictive Toxicology (NIEHS grant 1U19ES019528-01) and the NSF ERC Center for Environmental Implications of Nanotechnology at UCLA (NSF:EF-0820117). C.E.A. was supported by IGERT Fellowship Grant NSF DGE-0504276, and E.C.C. and N.J.C. were supported by NSF IGERT grant DGE- 0549500. T.N.H. was supported by NSF Nanoscience and Microsystems REU program (grant DMR-0649132) at the University of New Mexico Center for Micro-Engineered Materials. N.J.C. and D.N.P. were supported by NSF PREM/DMR 0611616. R. Lee provided guidance for imaging protocols and FRAP experiments, M. Aragon created schematic diagrams, R. Sewell carried out nitrogen sorption experiments and Y.-B. Jiang carried out TEM imaging. Cryogenic TEM was carried out at Baylor College of Medicine (Houston, TX) by C. Jia-Yin Fu, H. Khant and W. Chiu. Some images in this paper were generated in the University of New Mexico Cancer Center Fluorescence Microscopy Facility, supported by NCR, NSF and NCI as detailed at <http://hsc.unm.edu/crtc/microscopy/Facility.html>. Data were generated in the Flow Cytometry Shared Resource Center supported by the University of New Mexico Health Sciences Center and the University of New Mexico Cancer Center. Sandia is a multiprogramme laboratory operated by Sandia Corporation, a wholly owned subsidiary of Lockheed Martin Company, for the US Department of Energy's National Nuclear Security Administration under contract DE-AC04-94AL85000.

## Author contributions

C.E.A. engineered protocells for targeted delivery, carried out most experiments, analysed data and wrote the manuscript; E.C.C. assisted with experiment coordination, data analysis and manuscript preparation; G.K.P. carried out confocal fluorescence microscopy imaging; D.P. synthesized and characterized multimodal particles; P.A.B. carried out FRAP experiments; T.N.H. assisted with DOX capacity and release studies; J.L. contributed to the development of the original protocol construct; N.J.C. developed the emulsion processing necessary to synthesize multimodal particles; B.P. and M.B.C. carried out flow cytometry experiments; X.J. synthesized unimodal particles; D.R.D. carried out small-angle neutron scattering experiments and analysed nitrogen sorption data; D.N.P. supervised development of the multimodal particles; D.G.E. supervised FRAP experiments; A.N.P. suggested the FRAP experiment and aided in its interpretation; P.N.D., C.L.W., B.C., W.W. and D.S.P. provided intellectual oversight for delivery experiments involving drugs, siRNA and protein toxins; C.J.B. conceived of the protocol construct, provided overall intellectual guidance, carried out final edits of the manuscript and is principal investigator of the main supporting grants.

## Additional information

The authors declare no competing financial interests. Supplementary information accompanies this paper on [www.nature.com/naturematerials](http://www.nature.com/naturematerials). Reprints and permissions information is available online at <http://npg.nature.com/reprintsandpermissions>. Correspondence and requests for materials should be addressed to C.E.A. or C.J.B.

## The targeted delivery of multicomponent cargos to cancer cells by nanoporous particle-supported lipid bilayers

Carlee E. Ashley, Eric C. Carnes, Genevieve K. Phillips, David Padilla, Paul N. Durfee, Page A. Brown, Tracey N. Hanna, Juewen Liu, Brandy Phillips, Mark B. Carter, Nick J. Carroll, Xingmao Jiang, Darren R. Dunphy, Cheryl L. Willman, Dimiter N. Petsev, Deborah G. Evans, Atul N. Parikh, Bryce Chackerian, Walker Wharton, David S. Peabody and C. Jeffrey Brinker

*Nature Materials* **10**, 389–397 (2011); published online 17 April 2011; corrected online 10 May 2011.

In the version of this Letter originally published, in Fig. 1 a double bond in the maleimide cycle of the crosslinker molecular structure was missing; the definition of the SP94 peptide in the text should have read H<sub>2</sub>N-SFSIIHTPILPLGGC-COOH; and in Fig. 6a the lowest value of the right-hand *y* axis should have read 10<sup>6</sup>. These errors have now been corrected in the HTML and PDF versions.

## DRUG DELIVERY

# One nanoparticle, one kill

By wrapping a ligand-functionalized lipid membrane around a silica core, nanoparticles with a fluid surface are created. These combine unprecedented specificity in binding to cancer cells with the combinatorial delivery of drug cocktails.

Darrell J. Irvine

Nanoparticles capable of specifically binding to target cells and delivering high doses of therapeutic compounds are much sought after in materials science applied to medicine. Such materials could be transforming for cancer chemotherapy and a variety of other diseases, by making therapeutic delivery into disease cells more efficient while lowering the exposure of healthy tissue to toxic side effects<sup>1,2</sup>. The complexity of this engineering challenge can be appreciated by considering some of the properties an ideal targeted nanoparticle drug carrier would exhibit, including the capability of carrying high levels of multiple, diverse molecular cargos, circulating in the blood for extended periods without elimination by the immune system and binding only to target cells while avoiding other cells. A number of nanoparticle-based therapeutics are now in use in the clinic, many of which are based on liposomes — vesicles comprising a lipid bilayer surrounding an aqueous core — which have low immunogenicity, excellent safety profiles in humans and established approaches for clinical-scale manufacturing<sup>3</sup>. However, no targeted nanoparticle system has yet been approved by the US Food and Drug Administration, reflecting in part the complexity of designing particles that can meet all of the design criteria of targeted drug delivery. Attacking this problem head on, Ashley *et al.*<sup>4</sup> describe in *Nature Materials* a new type of composite nanoparticle — a hybrid between liposomes and nanoporous silica nanoparticles. The properties engineered into this system elegantly synergize to approach the goal of an ideal targeted-delivery agent.

Despite their attractive features, the physical properties of liposomes needed to obtain efficient drug loading and stable entrapment of cargo compounds may be in conflict with the properties of carriers that would be optimal for targeted drug delivery. Targeted delivery is achieved by functionalizing the surface of nanoparticles with ligands (proteins, nucleic acids or

small molecules) that will bind to specific molecules on target cells while avoiding nonspecific binding to other cells, blood or tissue components (Fig. 1; ref. 2). It has been shown how decoration of particles with multiple copies of such targeting ligands can increase the avidity of particles for target-cell binding, via the cooperative nature of multivalent binding to cell-surface receptors<sup>5–7</sup>. Unfortunately, nanoparticles with many identical copies of a molecular motif displayed on their surface structurally resemble viruses, and the immune system has evolved to strongly respond to such repeat chemical patterns. (In fact, nanoparticles displaying many copies

of an antigen make excellent vaccines<sup>8</sup>.) Thus, increasing the density of targeting ligands raises the concern that an immune response will be raised against the carrier. High-avidity binding to target cells could be achieved with lower densities of targeting ligand (provided that these ligands were mobile on the particle surface) capable of clustering to bind multivalently to cell-surface receptors (Fig. 1). Liposomes are uniquely well-suited to provide this kind of mobile ligand display: phospholipid bilayers can either exist in a gel phase, where the lipids are essentially arrested with little two-dimensional mobility in the plane of the bilayer, or a fluid phase, where the lipids

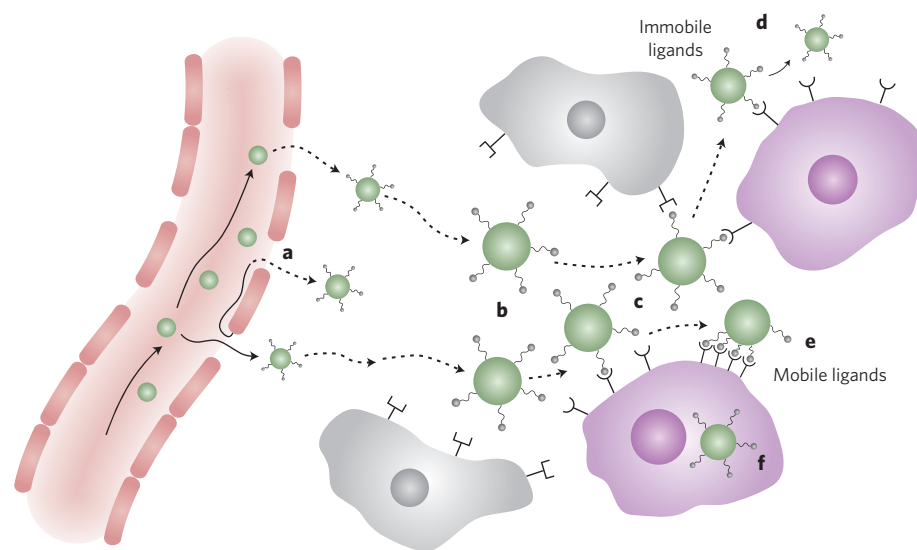


**Figure 1** | A schematic outlining multivalent targeting in nanoparticle drug delivery. Drug-loaded nanoparticles carrying therapeutics to tumour sites undergo a multistep process to achieve their therapeutic goal, beginning with extravasation from leaky tumour vessels (a), diffusion past non-target cells lacking receptors for the targeting ligand (b) and initial binding to receptors on target (for example, tumour) cells (c). Particles carrying low densities of targeting ligands on their surface are less likely to elicit an immune response or bind nonspecifically to non-target cells. However, if low-density ligands are immobile on the two-dimensional surface of the particle, multivalent binding to the target cell may not be possible and the lifetime of binding to the target cell may be too short to achieve internalization (d). In contrast, when ligands can diffuse over the two-dimensional particle surface, initial binding to targets can be followed by cooperative engagement of additional receptors as ligands diffuse into the particle/cell interface (e). This can lead to near-irreversible binding and rapid particle internalization for drug delivery into the cell (f).

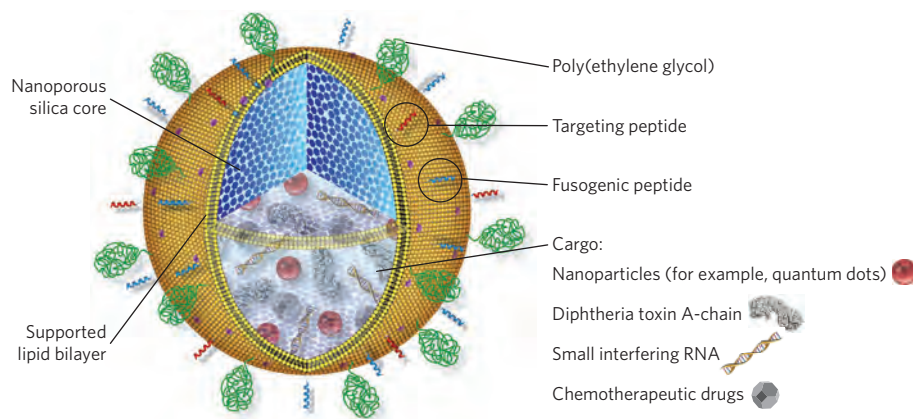


**Figure 2** | The design of lipid-bilayer-wrapped nanoporous silica, termed protocells. Nanoporous silica cores are loaded with multivariate drug cargos by adsorption to the silica matrix. The drug-loaded core is then enveloped by a single lipid bilayer, which is further functionalized with poly(ethylene glycol) (to reduce nonspecific interactions with its environment), peptides (to direct binding to distinct target cells) and pH-responsive peptides, which cause disruption of endosomes and the bilayer coating on particle internalization into acidic intracellular compartments, allowing drug delivery into the cytosol of the target cell. Figure adapted from ref. 4.

diffuse freely in the plane of the membrane. Targeting ligands anchored at a low surface density to the lipids of fluid-phase liposomes could thus readily achieve high-avidity binding via clustering, in theory. But here enters the design challenge: the liposomal compositions most favoured for drug delivery are generally rigid gel-phase vesicles, because fluid-phase liposomes have membranes that are poorly stable in the presence of blood components and are too permeable to be stably loaded with high levels of drug cargos<sup>3</sup>.

Ashley *et al.* report a solution to this challenge by wrapping fluid-phase lipid membranes around a drug-loaded nanoporous silica core to create hybrid particles they dub 'protocells' (Fig. 2). They demonstrate that the lipid membranes of these particles retain both high in-plane two-dimensional fluidity and high stability against destabilization in the presence of blood components or leakage of drug cargos from the silica core. This ideal combination of properties is proposed to arise from gradients in adhesion and membrane tension developed in the bilayer as it is stretched over alternating nanoscale patches of silica and pure water at the surface of the nanoporous silica core. The result is both an increase in relative two-dimensional fluidity of the membranes and a suppression of nanoscale fluctuations in the bilayer topology, compared with liposomes with the same membrane composition. These factors combine to allow ligand-decorated protocells to achieve avid binding to target cells with low densities of targeting ligand, conditions where off-target binding is also

lowered and immunogenicity of the particle is minimized. Ashley *et al.* impressively show that protocells have 100-fold greater specificity in target-cell binding than equivalent fluid-phase liposomes, suggesting that the suppression of bilayer fluctuations by the protocells' structure may be a key part of their efficient high-avidity binding to cells.

Another key issue in cancer drug delivery is that combinations of drugs are used clinically to maximize therapeutic efficacy while minimizing the potential for drug resistance. However, delivery of drug cocktails within liposomes remains a challenge, particularly for drug combinations with disparate physical properties such as charge, polarity and molecular weight. Here, the nanoporous silica core in the protocells plays a second key role (Fig. 2). The protocells can adsorb combinations of diverse drug cargos (quantum dots, small molecules and oligonucleotides) into their nanoporous silica cores, with reversible binding to the silica providing the means to soak up high levels of each drug cargo before enveloping the particle with its lipid shell. Strikingly, adsorption-mediated drug loading in the particle cores led to 1,000-fold greater doses of the common chemotherapy drug doxorubicin on a per-particle basis, compared with liposomes prepared by clinically employed methods. Silica binding probably also contributes to stable retention of these drug cargos following particle synthesis. It is then shown that these combinatorial cargos can be efficiently delivered into the cytosol or

nucleus of target cells 'on cue' following internalization, by including low densities of an endosome-disrupting peptide in the surface bilayer along with their targeting ligand.

Putting these synergistic features of enhanced specificity in targeted cell binding and combinatorial high-level drug loading together, Ashley *et al.*<sup>4</sup> finally demonstrate that targeted protocells carrying a cocktail of doxorubicin along with two other potent chemotherapeutics (5-fluorouracil and cisplatin) are so potent that a single particle on average per cell is sufficient to kill a model hepatic carcinoma cell; the efficient targeting allows these cells to be eliminated in cell culture under conditions that leave control healthy liver cells with >90% viability.

The experiments presented here are all *in vitro* and the degree to which this hybrid platform for drug delivery can advance therapeutic efficacy will need to be tested in animal models, where the complexity of events leading up to encounter of a nanoparticle with its target cell may have a significant impact on the ultimate outcome. If technically sound *in vivo*, it will also remain to be seen if particles with a large number of individual components as used here (PEGylation, targeting ligands, fusogenic peptides and multiple drug cargos) can be successfully translated to the clinic, from a manufacturing and intellectual-property perspective. However, this work offers the tantalizing prospect of taking highly potent yet toxic chemotherapy cocktails in use in the clinic and better focusing their action on the malignant cells for which they were intended. □

Darrell J. Irvine is in the Department of Biological Engineering, the Department of Materials Science and Engineering and the Koch Institute for Integrative Cancer Research, MIT, Cambridge, Massachusetts 02139, USA, and the Ragon Institute of Massachusetts General Hospital, MIT and Harvard University, Boston, Massachusetts 02129, USA. He is also an investigator of the Howard Hughes Medical Institute, Maryland 20815, USA. e-mail: djirvine@MIT.EDU

## References

1. Davis, M. E., Chen, Z. G. & Shin, D. M. *Nat. Rev. Drug Discov.* **7**, 771–782 (2008).
2. Farokhzad, O. C. & Langer, R. *ACS Nano* **3**, 16–20 (2009).
3. Torchilin, V. P. *Nat. Rev. Drug Discov.* **4**, 145–160 (2005).
4. Ashley, C. E. *et al.* *Nature Mater.* doi:10.1038/nmat2992 (2011).
5. Basha, S. *et al.* *Proc. Natl Acad. Sci. USA* **103**, 13509–13513 (2006).
6. Ho, K., Lapitsky, Y., Shi, M. & Shoichet, M. S. *Soft Matter* **5**, 1074–1080 (2009).
7. Poon, Z. *et al.* *Angew. Chem. Int. Ed. Engl.* **49**, 7266–7270 (2010).
8. Taneichi, M. *et al.* *J. Immunol.* **177**, 2324–2330 (2006).

Published online: 17 April 2011